HHS Public Access

Author manuscript

ACS Appl Mater Interfaces. Author manuscript; available in PMC 2018 November 19.

Published in final edited form as:

ACS Appl Mater Interfaces. 2018 April 25; 10(16): 13953–13962. doi:10.1021/acsami.8b00068.

Spray-Processed Composites with High Conductivity and Elasticity

Mert Vural[†], **Adam M. Behrens**[‡], **Wonseok Hwang**[†], **Joseph J. Ayoub**[†], **Dalton Chasser**[‡], **Arthur von Wald Cresce**[‖], **Omar B. Ayyub**[‡], **Robert M. Briber**[†], and **Peter Kofinas**[*,§]

[†]Department of Materials Science and Engineering, University of Maryland, College Park, Maryland 20742, United States

[‡]Fischell Department of Bioengineering, University of Maryland, College Park, Maryland 20742, United States

[§]Department of Chemical and Biomolecular Engineering, University of Maryland, College Park, Maryland 20742, United States

[‖]Electrochemistry Branch, Sensor and Electron Devices Directorate, Power and Energy Division, U.S. Army Research Laboratory, Adelphi, Maryland 20783, United States

Abstract

Highly conductive elastic composites were constructed using multistep solution-based fabrication methods that included the deposition of a nonwoven polymer fiber mat through solution blow spinning and nanoparticle nucleation. High nanoparticle loading was achieved by introducing silver nanoparticles into the fiber spinning solution. The presence of the silver nanoparticles facilitates improved uptake of silver nanoparticle precursor in subsequent processing steps. The precursor is used to generate a second nanoparticle population, leading to high loading and conductivity. Establishing high nanoparticle loading in a microfibrous block copolymer network generated deformable composites that can sustain electrical conductivities reaching 9000 S/cm under 100% tensile strain. These conductive elastic fabrics can retain at least 70% of their initial electrical conductivity after being stretched to 100% strain and released for 500 cycles. This composite material system has the potential to be implemented in wearable electronics and robotic systems.

Graphical Abstract

[*]**Corresponding Author** kofinas@umd.edu.

Author Contributions

The manuscript was written through contributions of all authors. All authors have given approval to the final version of the manuscript.

Notes

The authors declare no competing financial interest.

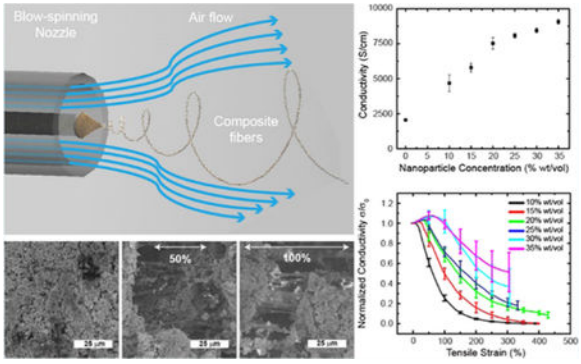

Keywords

elastic conductors; block copolymer composites; solution blow spinning; flexible electronics; wearables

INTRODUCTION

Materials with the ability to maintain high electrical conductivity under large deformations are necessary for the fabrication of stretchable electrical circuits with high performance and energy efficiency. Specifically, materials for connecting a variety of different rigid electric components on deforming substrates need to sustain electrical conductivities exceeding 1000 S/cm under tensile strain above 100% for applications in epidermal wearable devices, epidermal electronics, and robotics.[1–3] As interconnects, elastic conductors have been utilized for stretchable electronic devices, including displays,[4] solar cells,[5] supercapacitors,[6] batteries,[7] radio-frequency antennas,[8–10] smart textiles,[11–13] and epidermal sensors.[14–16]

The inherently brittle nature of most conductive materials and poor electrical properties of elastomers necessitate the use of composites in the development of elastic conductors with high electrical conductivity.[17,18] Recent efforts toward developing intrinsically stretchable conductors using conductive polymers and macromolecular additives have led to conductive polymers blends that remain conductive under strain values exceeding 100%.[2,3,11,19] The applicability of conductive polymer blends is limited due to low electrical conductivity values, leading to the continued investigation of composite elastic conductors.[2,20–22] The most common approaches are liquid metal-filled channels within soft elastomer matrixes[8,23,24] or conductive networks composed of nanowires[25,26] or nanotubes[27,28] backfilled with an elastomeric component. In the first case, the liquid metal alloy is able to take the shape of channels fabricated in a soft elastomeric matrix. These elastic conductors have reliability concerns due to their extremely poor mechanical properties and risk of leakage of the conductive component.[17,23] Elastomer-backfilled conductive nanowire or nanotube networks have similar advantages and deficiencies with the ability to maintain high electrical conductivity at the expense of poor mechanical properties. In these materials, the large amount of the conductive component required for high conductivity leads to limited elongation at failure.[26,27,29–31] Certain limitations of these approaches have been resolved by patterning the metallic component in specific geometries, including springs,[32,33] wavy,[32,34–36] and fractal patterns.[37] These patterns are able to maintain high conductivities under

moderate strains but have finite maximum strains that arise from the limitations of the chosen geometry.[35,37]

More recently, elastic conductors made using composites that consist of elastomers and conductive nanoparticles have proven to be an effective means of developing high-performance materials for use in stretchable device applications.[9,38] Even though these materials require higher concentrations of the conductive component when compared to nanowires or nanotubes to establish conductivity, the spherical geometry provides improved particle mobility within the polymer matrix when undergoing strain.[17,39] Increased particle mobility allows these composites to maintain a large percentage of their initial conductivity under tension due to the dynamic formation of alternate conductive pathways during deformation. The elastic properties of these composites still considerably diminish with increasing nanoparticle content, which is required to reach high conductivity values.[39]

Using polymer fibers as the elastomeric portion of the composite has partially addressed this shortcoming.[9,38] Confining nanoparticles in a cylindrical geometry enables the composites to reach higher electrical conductivity values with the same filler content due to a lower percolation threshold.[9] The fiber network also provides a mechanism to establish alternative conductive pathways under tensile deformation through fiber rearrangement.[40] Elastic conductors based on polymer fiber networks have displayed a variety of material properties ranging from highly deformable materials with limited electrical conductivity[38] to highly conductive composites with strain-sensitive electrical properties.[9] The difficulties in achieving both a highly deformable and highly conductive material arise from nanoparticle localization at the fiber surface and/or low volumetric concentration of the nanoparticles in the composite.[9,38]

Here, we demonstrate solution-based fabrication of highly conductive composites that consist of block copolymer fiber networks and conductive nanoparticles. High nanoparticle loading is achieved by introducing silver nanoparticles into the fiber spinning solution. The presence of the silver nanoparticles facilitates improved uptake of silver nanoparticle precursor in subsequent processing steps. The precursor is used to generate a second nanoparticle population, leading to high loading and conductivity. Specifically, poly(acrylic acid)-capped silver nanoparticles (Ag−PAA nanoparticles) were synthesized using an aqueous synthesis method. The synthesized Ag−PAA nanoparticles were then dispersed in a solution of poly(styrene-*b*-isoprene-*b*-styrene) (SIS) block copolymer dissolved in tetrahydrofuran (THF). This solution is then deposited as a nonconductive polymer fiber network containing in-fiber Ag− PAA nanoparticles using a technique called solution blow spinning. This technique allows polymer fiber networks to be rapidly deposited on a substrate of interest, including synthetic and biological interfaces.[38,41] A second population of nanoparticles is introduced to the polymer−nanoparticle composite through the addition and nucleation of an organometallic precursor. The nucleation of secondary nanoparticle population leads to the formation of an interconnected network of conductive nanoparticles throughout the composite. The resulting material reaches a maximum initial conductivity value of 9000 ± 200 S/cm, which drops to 5100 ± 250 S/cm after 500 cycles at 100% strain. The high electrical conductivity of the composites can be attributed to the high silver nanoparticle concentration distributed in and around the elastomeric fiber matrix.

Additionally, the elastomeric fiber matrix helps sustain a significant portion of the electrical conductivity under cyclic tensile deformation by facilitating the formation of alternative conductive pathways.

EXPERIMENTAL SECTION

Synthesis of Poly(acrylic acid)-Capped Silver Nanoparticles.

Poly(acrylic acid) (PAA)-capped silver nanoparticles were synthesized using $AgNO_3$, monoethanolamine (MEA), and PAA. Initially, 100 mmol $AgNO_3$ (Sigma-Aldrich, 99%), 400 mmol MEA (Sigma-Aldrich, 99%), and 7.2 mL of PAA (Acros Organics, 50 wt % water solution) were dissolved in 75 mL of deionized water and stirred for 30 min. The solution was placed in an oil bath with temperature set to 60 °C and rigorously stirred for 2 h. The particles were precipitated using 250 mL of ethanol (Pharmco-Aaper, 99%) and washed several times with ethanol to remove excess or unreacted reagents. The resulting nanoparticles were dried under vacuum at 60 °C for 24 h.

Stretchable Conductor Fabrication.

Solution blow spinning solutions consisting of PAA-capped nanoparticles, poly(styrene-*b*-isoprene-*b*-styrene) (SIS; Sigma-Aldrich, 22% w/w styrene content), and tetrahydrofuran (THF; Fisher Scientific, 99.9%) were prepared and fed with a constant rate (10 mL/h) through the nozzle of the solution blow spinning apparatus (Figure 1a,b). The apparatus was constructed from a flat-tipped 18G needle (outer diameter = 1.27 mm, inner diameter = 0.838, and wall thickness = 0.216) syringe pump and compressed air-line. The air pressure was kept constant at approximately 345 kPa during the deposition process. The nonconductive composite mat composed of block copolymer fibers and Ag−PAA nanoparticles was deposited on a mesh. This nonconductive composite mesh was then immersed into an organometallic solution that consists of silver trifluoroacetate (STFA; Sigma-Aldrich, 98%) and ethanol (Pharmco-Aaper, 99%) for 30 min. The STFA concentration in ethanol was 25% (w/v) for each composite mat. The swollen mat was then vacuum dried in a desiccator. The nucleation of additional silver nanoparticles was initiated by the addition of a reducing solution that consists of hydrazine hydrate (50% v/v; Sigma-Aldrich, 50−60%), deionized water (25% v/v), and ethanol (25% v/v). The resulting conductive composites were rinsed thoroughly with water to wash away any unbound nanoparticles and dried under vacuum for 24 h.

Characterization.

Scanning electron microscopy (SEM; Hitachi SU-70) and transmission electron microscopy (TEM; JEOL 2100F) were used to characterize the structure of the block copolymer nanoparticle composites. The TEM sample used for cross-section analysis was prepared using a cryomicrotome (Leica EM UC-6) with a 100 nm sample thickness. Size distributions (Figure S1a,b) of silver nanoparticles are reported as the average of nanoparticle diameter from three different TEM images ($n = 150$). A dynamic mechanical analyzer (TA Instruments Q800) was used to characterize the mechanical properties of the elastic conductors. Energy dissipation was calculated from the area of the hysteresis loops of cyclic stress/strain curves for both SIS fiber mats and conductive composites. Thermogravimetric

analysis (TGA) was performed under nitrogen to identify the volume fraction of silver in the composite (Netzsch F3 Jupiter). The electrical conductivity of the elastic conductor samples was measured using a homemade automated four-point probe measurement system. This system consists of a probe assembly with spring-loaded contact probes separated by a 2 mm distance (interprobe distance is 2 mm) and a Keithley 2400 Sourcemeter. The normalized conductivity measurements under mechanical strain were performed using a custom-built electromechanical characterization system (Figure S2). This system consists of a motorized stage and clamps manufactured with a built-in four-point probe measurement system (interprobe distance of 5 mm). These probes (two probes for each clamp) are located beyond the region of deformation for the conductive samples, which facilitates stable electrical contacts during the course of tensile deformation experiments. Measurement probes are connected to an Agilent 34420A Micro-Ohm Meter and a National Instruments PXI4065 Digital Multimeter for acquiring multiple readouts of resistivity. National Instruments digital multimeter allows for digitalization of acquired data, whereas Agilent system is used to monitor the experiment and confirm the accuracy of the acquired data.

RESULTS AND DISCUSSION

Elastic conductors were fabricated by a multistep process starting with preparation of pristine or composite polymer (SIS) solutions containing various concentrations of poly(acrylic acid)-capped silver nanoparticles (Ag−PAA nanoparticles). This is followed by subsequent deposition of SIS or composite solutions through solution blow spinning to generate fibrous materials (Figure 1a(i),(ii),b(i),(ii)). A free-standing nonconductive composite polymer fiber mat containing Ag−PAA nanoparticles is shown in Figure 1b(ii) demonstrating similar morphology to a SIS polymer fiber mat shown in Figure 1a(ii). Polymer and composite fiber generation through this method only requires a simple apparatus, highpressure gas source, and a viscous spinning solution (Figure 1a(i),b(i)).[42,43] Similar to other solution-processed fiber spinning techniques, fiber geometry is achieved after exceeding a critical solution concentration, resulting in polymer chain overlap.[43] The inclusion of inorganic nanoparticles into the spinning solution can alter optimal spinning parameters.[44] The use of poly(acrylic acid) capping on silver nanoparticles enabled dispersion of nanoparticles in the spinning solution, allowing for the generation of fiber morphologies up to a critical nanoparticle concentration. The solutions prepared with Ag −PAA nanoparticle concentrations exceeding 35% (w/v) did not generate a fibrous morphology under the same deposition conditions. This limit can be attributed to high solution viscosity leading to clogging of the spinning apparatus.

After polymer deposition, the fiber mats were immersed in an ethanol solution containing an organometallic precursor. Both SIS fiber mats and the composite fiber mats swelled drastically (190 ± 20, 310 ± 30% increase in weight after swelling) without releasing silver nanoparticles. The weight of the SIS and composite fiber mats only increased by 10% when the organometallic precursor was not present in the ethanol solution. This large difference in swelling is attributed to the interaction between the silver ions present in the organometallic precursor solution and the unsaturated hydrocarbons contained in the isoprene block of SIS.[45] The unsaturated (C ==C) double bond donates π electrons to occupy free s and p orbitals of Ag^+, which results in formation of weak chargetransfer complexes between the polymer

and the precursor.[9,45] Similarly, negatively charged poly(acrylic acid) (PAA)-capped silver nanoparticles can interact with Ag^+, which also helps to facilitate the absorption of silver precursor on the composite fibers.[35] In the final step, a conductive network of silver nanoparticles was formed throughout the fiber mats by the introduction of a reducing solution (Figure 1a(iii),b(iii)).

Structural characterization performed by scanning electron microscopy (SEM) showed that the SIS mats and composite mats are composed of fibers with similar diameters (1.66 ± 0.7 and 2.12 ± 0.8 μm, Figure 2a,b). This indicates the ability to form a fiber network is maintained after addition of Ag−PAA nanoparticles into the spinning solution up to a concentration of 35% (w/v) (Figure 2b). The Ag−PAA nanoparticles form chainlike assemblies in the fibers; this is attributed to the direction of flow during the solution blow spinning process (Figure 2b, inset). After the introduction of the organometallic precursor and subsequent nucleation by the addition of a hydrazine hydrate solution, a silver nanoparticle network forms in and around SIS and composite fibers generating conductive pathways (Figure 2c,d). This nanoparticle network covers the entire surface of the composite fibers prepared from a spinning solution with 35% (w/v) Ag−PAA nanoparticle concentration (Figure 2d). For these conductive composites, it becomes difficult to identify the fiber morphology after nucleation. However, fibers remain visible for composites prepared using block copolymer fiber mats that do not contain Ag−PAA nanoparticles (Figure 2c). This is potentially due to higher accumulation of precursor solution for fiber mats containing infiber Ag−PAA nanoparticles (310 ± 30% weight increase) relative to block copolymer mats deposited using SIS alone (190 ± 20% weight increase).

TGA analysis performed on the composite polymer fiber mats demonstrated that 35% (w/v) Ag−PAA nanoparticle concentration in spinning solution leads to composites with an Ag −PAA nanoparticle concentration of 22% (w/w) (Figure 3a). The TGA characterization of the elastic conductors after the introduction and reduction of the silver precursor showed silver concentrations reach 81% (w/w) (27.4% v/v) (Figure 3b). This silver concentration is much higher than the silver content in elastic conductors fabricated from SIS fiber mats without the initial presence on in-fiber Ag−PAA nanoparticles (52% w/w, 8.8% v/v) (Figure 3a,b). It is important to highlight that the sum of silver concentrations of composite fiber mats (22% w/w) and elastic conductors prepared using SIS fiber mats (52% w/w) could not reach the silver concentration of elastic conductors fabricated using composite fiber mats (81% w/w). This is a clear indication that presence of Ag−PAA nanoparticles facilitates improved silver nucleation in these composite materials. The cross-sectional TEM image of these elastic conductors revealed that silver nanoparticles also nucleate between the existing Ag−PAA nanoparticles in the fiber cross section (Figures 2d, inset and S1c). This is in contrast to the SIS fiber mats not containing Ag−PAA nanoparticles, in which nucleation is limited at the fiber surface (Figure 2c, inset). This result supports that inclusion of Ag− PAA nanoparticles in the polymer solution facilitates silver nanoparticle nucleation in block copolymer fibers. The size distributions of Ag−PAA nanoparticles and silver nanoparticles in elastic conductors were measured using cross-sectional TEM images as 150 ± 50 and 20.6 ± 14.2 nm, respectively (Figures 2d, inset and S1c).

The mechanical properties of elastic conductors prepared using spinning solutions with different Ag−PAA nanoparticle concentrations were characterized to investigate the influence of nanoparticle content on tensile modulus and elongation at break. Increased Ag −PAA nanoparticle concentration in the spinning solutions resulted in more brittle composites with lower elongation at break (Figure 3c) and higher tensile modulus (Figure 3d). The effect of Ag−PAA nanoparticle concentration on overall conductivity and strain dependence of electrical properties was also assessed (Figure 4a). Maximum conductivity values reached 9000 ± 200 S/cm when testing composite fiber mats with the highest Ag −PAA nanoparticle concentration (35% w/v in the spinning solution) that could be deposited in a fibrous morphology. Electrical conductivity measurements during tensile deformation revealed that these elastic conductors with high volumetric fraction of silver (27.4% v/v) can maintain 52% of their initial conductivity (σ_0) prior to mechanical failure at 302% strain (Figure 4b). The electrical conductivity dependence on tensile strain increased drastically with decreasing Ag−PAA nanoparticle concentration. This can be observed for elastic conductors fabricated using spinning solutions with only 10% w/v Ag−PAA nanoparticle concentration, which lost 99% of their initial conductivity at 300% strain (Figure 4b). The elastic conductors with high conductive filler fraction (27.4% v/v) demonstrate nearly stable electrical conductivity up to 100% strain (Figure 4b). It is important to note that the ability to maintain electrical conductivity up to 100% strain can help improve energy efficiency and circuit design for flexible electronics as the resistivity of interconnects remains stable.[2,3] Additionally, the electrical conductivity of these elastic conductor composites is similar or superior to highly conductive stretchable composites with similar filler concentration (27.4% v/v). This analysis highlights the impact of the fibrous structure on the percolation of nanoparticles (Figure 4c).[30,39,46] For strain values exceeding 100%, the electrical conductivity of these elastic conductors decreases less drastically compared to that of existing stretchable conductive composites (Figure 4c). This electromechanical behavior allows this composite material to sustain electrical conductivity values significantly higher than 1000 S/cm under 300% strain. A material exceeding these benchmarks can enable operation of electronic systems under extreme deformation conditions for applications in robotics.[1]

A small increase in electrical conductivity with increasing tensile strain was observed for elastic conductors at strain values up to 50%. This can be explained by strain-mediated stiffening effects observed in composite fibers and fiber network structures.[39,47,48] The diameter of composite fibers filled with conductive nanoparticles decreases with increasing strain, which may increase the number of particle-to-particle contacts.[47,48] Because of increased number of connections between particles, the elastic conductors can facilitate higher number of conductive pathways leading to improved electrical conductivity.[39,47,49] The electrical conductivities of fiber, nanowire, and nanotube networks have been shown to increase under tensile strain due to increased number of contacts.[40,48] This effect can persist until the complete alignment of the network structure in the direction of applied strain. For strain values exceeding 50%, elastic conductors with filler concentrations higher than the percolation threshold (16% v/v) follow the percolation theory that defines the change in electrical conductivity with applied strain (Figures 4d and S3).[39] Beyond 150% strain, the electromechanical behavior of these composites begins to diverge from percolation theory as

the geometry of the composite samples alters due to formation of ruptures and holes (Figure 4d).

Changes in electrical conductivity under cyclic deformation were also evaluated by deforming elastic conductors with various Ag−PAA nanoparticle concentrations to 100% strain for 500 cycles (Figure 4e,f). The elastic conductors composed of high concentrations of Ag−PAA nanoparticles (35, 30, 25 w/v in the spinning solution) maintained at least 70% of their initial conductivity after cyclic testing (Figure 4e). This is in contrast to elastic conductors that consist of low concentrations of Ag−PAA nanoparticles (20, 15, 10 w/v in the spinning solution), which decreased more drastically with consecutive tensile strain cycling (Figure 4e). Electrical conductivity values at 100% strain for elastic conductors with low Ag−PAA nanoparticle content deteriorated to below 20% of their initial conductivity after 10 cycles of tensile deformation up to 100% strain (Figure 4f).

Further mechanical characterization of the conductive composites was performed using stress/strain cycling to evaluate the extent of plastic deformation (Figure 5a,b). The elastic conductors prepared using higher Ag−PAA nanoparticle concentrations demonstrated a slightly lower elastic recovery in comparison to that of elastic conductors fabricated using low Ag−PAA nanoparticle concentrations (Figures 5a,b and S4). Energy dissipation values were calculated from the area under the stress/strain curve at each maximum strain value. Linear correlations of energy dissipation with increasing strain correspond to structural deformation mechanisms (Figures 5c,d and S5).[38,50,51] Elastic conductors fabricated from composite mats with low Ag−PAA nanoparticle concentrations (20, 15, 10% w/v in the spinning solution) demonstrated three distinct regions corresponding to strain-induced structural changes. These changes have been observed in fibrous polymer−nanoparticle composites (Figures 5c and S5a,b).[38] The initial structural changes originate from breakage of fiber-to-fiber junctions established during silver nanoparticle nucleation up to tensile strain of 50%. As the fibers gain the ability to independently rearrange for strain values higher than 50%, the structural deformations generate a less drastic increase in energy dissipation along the second strain region until reaching 100% strain. Individual fiber deformation dominates the structural deformation for strain values exceeding 100%, resulting in an increased rate of energy dissipation due to loss of filler-to-polymer and filler-to-filler contact. In contrast, elastic conductors prepared using high Ag−PAA nanoparticle concentrations (35, 30, 25% w/v in the spinning solution) exceeding percolation threshold demonstrated a single linear correlation region with higher slope. This continuous increase in energy dissipation can be explained by strain softening effect for composites with high filler concentration. This effect occurs at strain values higher than elastic tensile deformation limit.[52,53] The shift in energy dissipation behavior with applied strain indicates that the nonlinear elastic behavior is dominated by deformation mechanisms originating from the changes in particle-to-polymer and particle-to-particle contact (Figures 4d and S5c,d).[53]

Electron microscopy was used to further investigate the difference in deformation mechanisms between low and high nanoparticle loading composites. Elastic conductors with differing Ag−PAA nanoparticle concentrations were imaged under 0, 50, and 100% strain to visualize differences in the progression of the material's morphology under strain (Figure 6). The SEM images of elastic conductors assembled using fiber spinning solutions with 10%

w/v Ag−PAA nanoparticles show that these composites demonstrate the deformation mechanics of fibrous polymer−nanoparticle composites (Figure 6a−c).[38] The SEM images of these elastic conductors at 50% strain show that fibers orient along the direction of tensile deformation by breaking fiber-to-fiber junctions as the majority of the nanoparticles covering the surface remains intact (Figure 6b). At 100% strain, the fibers orient completely in the direction of tensile strain and surface coverage of nanoparticles becomes discontinuous, indicating the onset of individual fiber deformation (Figure 6c). The fibrous network structure of elastic conductors prepared using fiber spinning solutions with 35% w/v Ag−PAA nanoparticle concentration is not discernible at 0% strain as the surface is completely covered with silver nanoparticles (Figure 6d). At 50% strain, the fiber network structure becomes visible among voids that are formed during deformation (Figure 6e). Nearly all of the composite fibers are aligned in the direction of applied strain after the elastic conductor is stretched to 50% strain. The SEM images of these elastic conductors under 100% strain indicate that the conductive fiber network detaches into individual fibers with discontinuous nanoparticle coverage upon further tensile deformation. In light of this structural characterization, it is apparent that fiber rearrangement in these composites governs structural deformation up to 50% strain. For strain values larger than 50%, elastic conductors act as regular polymer−nanoparticle composites as the influence of fibrous network on electrical properties becomes negligible. At strain values exceeding 50%, fibers either align in the direction of applied strain or they form compact bundles that cannot disentangle to facilitate higher strain values without plastic deformation. This deformation mechanism explains the electromechanical behavior of elastic conductors at strain values larger than 50%. It also supports the single mode of structural change, loss of particle-to-particle contacts, shown previously by a linear increase in energy dissipation with strain.

To visualize these structural deformations of the elastic conductors with high Ag−PAA nanoparticle concentration in a broader perspective, low-magnification SEM images were acquired under strain values of 0, 25, 50, and 100% (Figure S6). The unstrained condition shows a composite surface densely covered by silver nanoparticles (Figure S6a). As this composite is stretched to slightly above its elastic deformation limit, it begins to form voids. However, the majority of the composite still remains connected with nanoparticles (Figure S6b). As the strain value reaches 50%, the number of voids between large composite blocks increases (Figure S6c). The conductive fiber networks, which were previously demonstrated in the highmagnification SEM images, connect these large composite segments during deformation (Figure S6c). This highlights the influence of fiber network on the strain-dependent electrical properties of elastic conductors at strain values exceeding the elastic deformation limit (20% strain). Further stretching (strain values of 100%) resulted in a morphology that consists of smaller, segmented regions, connected with individual fibers with discontinuous nanoparticle coverage (Figures 6f and S6d). This structural evolution is observed throughout the entire composite, as examined through SEM. In terms of electrical properties, this structure is more analogous to large composite segments dispersed in a matrix as the fibers connecting the composite blocks have discontinuous nanoparticle coverage resulting in conductivity loss. This structural outline explains the unique electrical and electromechanical properties of these elastic conductors with dual nanoparticle networks.

CONCLUSIONS

We have demonstrated solution-processed elastic conductors with high nanoparticle loading by employing silver nanoparticles (150 ± 50 nm) in a spinning solution to generate a fibrous composite template for initiating a secondary silver nanoparticle nucleation (20.6 ± 14.2 nm). The resulting materials reach conductivity values of 9000 S/cm that only decrease to 5100 S/cm after 500 cycles of 100% strain. The high electrical conductivity of these composite materials originates from the high volumetric fraction of conductive fillers (27.4% v/v) that are assembled in and around the elastomeric fiber matrix of SIS. The random fibrous network structure of these composites stemming from an elastomeric fiber matrix also allows them to sustain a significant portion of their electrical conductivity during cyclic tensile deformation. We have additionally demonstrated control over strain-dependent electrical properties of the elastic conductors by decreasing the Ag−PAA nanoparticle concentration employed in elastic conductors. This versatility enables adjusting material properties for specific applications.

Supplementary Material

Refer to Web version on PubMed Central for supplementary material.

ACKNOWLEDGMENTS

We acknowledge the support from the Nanoscale Imaging, Spectroscopy, and Properties Laboratory (NISPLab) at the University of Maryland Nanocenter.

Funding

This work was supported by AOARD grant #FA23861714051.

REFERENCES

(1). Lu N; Kim D-H Flexible and stretchable electronics paving the way for soft robotics. Soft Robotics 2014, 1, 53–62.

(2). Wang Y; Zhu C; Pfattner R; Yan H; Jin L; Chen S; Molina-Lopez F; Lissel F; Liu J; Rabiah NI; Chen Z; Chung JW; Linder C; Toney MF; Murmann B; Bao Z A highly stretchable, transparent, and conductive polymer. Science Adv 2017, 3, No. e1602076.

(3). Lipomi DJ; Vosgueritchian M; Tee BCK; Hellstrom SL; Lee JA; Fox CH; Bao Z Skin-like pressure and strain sensors based on transparent elastic films of carbon nanotubes. Nat. Nanotechnol 2011, 6, 788–792. [PubMed: 22020121]

(4). Sekitani T; Nakajima H; Maeda H; Fukushima T; Aida T; Hata K; Someya T Stretchable active-matrix organic light-emitting diode display using printable elastic conductors. Nat. Mater 2009, 8, 494–499. [PubMed: 19430465]

(5). Lipomi DJ; Tee BCK; Vosgueritchian M; Bao ZN Stretchable Organic Solar Cells. Adv. Mater 2011, 23, 1771–1775. [PubMed: 21491510]

(6). Hu L; Pasta M; Mantia FL; Cui L; Jeong S; Deshazer HD; Choi JW; Han SM; Cui Y Stretchable, porous, and conductive energy textiles. Nano Lett 2010, 10, 708–714. [PubMed: 20050691]

(7). Xu S; Zhang Y; Cho J; Lee J; Huang X; Jia L; Fan JA; Su Y; Su J; Zhang H; Cheng H; Lu B; Yu C; Chuang C; Kim TI; Song T; Shigeta K; Kang S; Dagdeviren C; Petrov I; Braun PV; Huang Y; Paik U; Rogers JA Stretchable batteries with self-similar serpentine interconnects and integrated wireless recharging systems. Nat. Commun 2013, 4, No. 1543.

(8). Kubo M; Li XF; Kim C; Hashimoto M; Wiley BJ; Ham D; Whitesides GM Stretchable Microfluidic Radiofrequency Antennas. Adv. Mater 2010, 22, 2749–2752. [PubMed: 20414886]

(9). Park M; Im J; Shin M; Min Y; Park J; Cho H; Park S; Shim MB; Jeon S; Chung DY; Bae J; Park J; Jeong U; Kim K Highly stretchable electric circuits from a composite material of silver nanoparticles and elastomeric fibres. Nat. Nanotechnol 2012, 7, 803− 809. [PubMed: 23178335]

(10). Song L; Myers AC; Adams JJ; Zhu Y Stretchable and Reversibly Deformable Radio Frequency Antennas Based on Silver Nanowires. ACS Appl. Mater. Interfaces 2014, 6, 4248–4253. [PubMed: 24593878]

(11). Matsuhisa N; Kaltenbrunner M; Yokota T; Jinno H; Kuribara K; Sekitani T; Someya T Printable elastic conductors with a high conductivity for electronic textile applications. Nat. Commun 2015, 6, No. 7461. [PubMed: 26109453]

(12). Lee J; Kwon H; Seo J; Shin S; Koo JH; Pang C; Son S; Kim JH; Jang YH; Kim DE; Lee T Conductive Fiber-Based Ultrasensitive Textile Pressure Sensor for Wearable Electronics. Adv. Mater 2015, 27, 2433–2439. [PubMed: 25692572]

(13). Gong S; Schwalb W; Wang YW; Chen Y; Tang Y; Si J; Shirinzadeh B; Cheng WL A wearable and highly sensitive pressure sensor with ultrathin gold nanowires. Nat. Commun 2014, 5, No. 3132. [PubMed: 24495897]

(14). Kim DH; Lu NS; Ma R; Kim YS; Kim RH; Wang SD; Wu J; Won SM; Tao H; Islam A; Yu KJ; Kim TI; Chowdhury R; Ying M; Xu LZ; Li M; Chung HJ; Keum H; McCormick M; Liu P; Zhang YW; Omenetto FG; Huang YG; Coleman T; Rogers JA Epidermal Electronics. Science 2011, 333, 838–843. [PubMed: 21836009]

(15). Dagdeviren C; Su YW; Joe P; Yona R; Liu YH; Kim YS; Huang YA; Damadoran AR; Xia J; Martin LW; Huang YG; Rogers JA Conformable amplified lead zirconate titanate sensors with enhanced piezoelectric response for cutaneous pressure monitoring. Nat. Commun 2014, 5, No. 4496. [PubMed: 25092496]

(16). Dagdeviren C; Shi Y; Joe P; Ghaffari R; Balooch G; Usgaonkar K; Gur O; Tran PL; Crosby JR; Meyer M; Su YW; Webb RC; Tedesco AS; Slepian MJ; Huang YG; Rogers JA Conformal piezoelectric systems for clinical and experimental characterization of soft tissue biomechanics. Nat. Mater 2015, 14, 728–736. [PubMed: 25985458]

(17). Park M; Park J; Jeong U Design of conductive composite elastomers for stretchable electronics. Nano Today 2014, 9, 244–260.

(18). Rogers JA; Someya T; Huang YG Materials and Mechanics for Stretchable Electronics. Science 2010, 327, 1603–1607. [PubMed: 20339064]

(19). Matsuhisa N; Inoue D; Zalar P; Jin H; Matsuba Y; Itoh A; Yokota T; Hashizume D; Someya T Printable elastic conductors by in situ formation of silver nanoparticles from silver flakes. Nat. Mater 2017, 16, 834–840. [PubMed: 28504674]

(20). Lipomi DJ; Lee JA; Vosgueritchian M; Tee BCK; Bolander JA; Bao Z Electronic Properties of Transparent Conductive Films of PEDOT:PSS on Stretchable Substrates. Chem. Mater 2012, 24, 373–382.

(21). Oh JY; Kim S; Baik H-K; Jeong U Conducting Polymer Dough for Deformable Electronics. Adv. Mater 2016, 28, 4455–4461. [PubMed: 26460551]

(22). Savagatrup S; Chan E; Renteria-Garcia SM; Printz AD; Zaretski AV; O'Connor TF; Rodriquez D; Valle E; Lipomi DJ Plasticization of PEDOT:PSS by Common Additives for Mechanically Robust Organic Solar Cells and Wearable Sensors. Adv. Funct. Mater 2015, 25, 427–436.

(23). Dickey MD; Chiechi RC; Larsen RJ; Weiss EA; Weitz DA; Whitesides GM Eutectic gallium-indium (EGaIn): A liquid metal alloy for the formation of stable structures in microchannels at room temperature. Adv. Funct. Mater 2008, 18, 1097–1104.

(24). Zhu S; So JH; Mays R; Desai S; Barnes WR; Pourdeyhimi B; Dickey MD Ultrastretchable Fibers with Metallic Conductivity Using a Liquid Metal Alloy Core. Adv. Funct. Mater 2013, 23, 2308–2314.

(25). Lee S; Shin S; Lee S; Seo J; Lee J; Son S; Cho HJ; Algadi H; Al-Sayari S; Kim DE; Lee T Ag Nanowire Reinforced Highly Stretchable Conductive Fibers for Wearable Electronics. Adv. Funct. Mater 2015, 25, 3114–3121.

(26). Xu F; Zhu Y Highly Conductive and Stretchable Silver Nanowire Conductors. Adv. Mater 2012, 24, 5117–5122. [PubMed: 22786752]

(27). Sekitani T; Noguchi Y; Hata K; Fukushima T; Aida T; Someya T A rubberlike stretchable active matrix using elastic conductors. Science 2008, 321, 1468–1472. [PubMed: 18687922]

(28). Kim KH; Vural M; Islam MF Single-Walled Carbon Nanotube Aerogel-Based Elastic Conductors. Adv. Mater 2011, 23, 2865–2869. [PubMed: 21495087]

(29). Amjadi M; Pichitpajongkit A; Lee S; Ryu S; Park I Highly Stretchable and Sensitive Strain Sensor Based on Silver Nanowire-Elastomer Nanocomposite. ACS Nano 2014, 8, 5154–5163. [PubMed: 24749972]

(30). Chun KY; Oh Y; Rho J; Ahn JH; Kim YJ; Choi HR; Baik S Highly conductive, printable and stretchable composite films of carbon nanotubes and silver. Nat. Nanotechnol 2010, 5, 853–857. [PubMed: 21113161]

(31). Liu ZF; Fang S; Moura FA; Ding JN; Jiang N; Di J; Zhang M; Lepro X; Galvao DS; Haines CS; Yuan NY; Yin SG; Lee DW; Wang R; Wang HY; Lv W; Dong C; Zhang RC; Chen MJ; Yin Q; Chong YT; Zhang R; Wang X; Lima MD; Ovalle-Robles R; Qian D; Lu H; Baughman RH Hierarchically buckled sheath-core fibers for superelastic electronics, sensors, and muscles. Science 2015, 349, 400–404. [PubMed: 26206929]

(32). Kim DH; Song JZ; Choi WM; Kim HS; Kim RH; Liu ZJ; Huang YY; Hwang KC; Zhang YW; Rogers JA Materials and noncoplanar mesh designs for integrated circuits with linear elastic responses to extreme mechanical deformations. Proc. Natl. Acad. Sci. U.S.A 2008, 105, 18675–18680. [PubMed: 19015528]

(33). Bagal A; Dandley EC; Zhao JJ; Zhang XA; Oldham CJ; Parsons GN; Chang CH Multifunctional nano-accordion structures for stretchable transparent conductors. Mater. Horiz 2015, 2, 486–494.

(34). Bowden N; Brittain S; Evans AG; Hutchinson JW; Whitesides GM Spontaneous formation of ordered structures in thin films of metals supported on an elastomeric polymer. Nature 1998, 393, 146–149.

(35). Ahn BY; Duoss EB; Motala MJ; Guo XY; Park SI; Xiong YJ; Yoon J; Nuzzo RG; Rogers JA; Lewis JA Omnidirectional Printing of Flexible, Stretchable, and Spanning Silver Microelectrodes. Science 2009, 323, 1590–1593. [PubMed: 19213878]

(36). Tybrandt K; Voros J Fast and Efficient Fabrication of Intrinsically Stretchable Multilayer Circuit Boards by Wax Pattern Assisted Filtration. Small 2016, 12, 180–184. [PubMed: 26618302]

(37). Fan JA; Yeo WH; Su YW; Hattori Y; Lee W; Jung SY; Zhang YH; Liu ZJ; Cheng HY; Falgout L; Bajema M; Coleman T; Gregoire D; Larsen RJ; Huang YG; Rogers JA Fractal design concepts for stretchable electronics. Nat. Commun 2014, 5, No. 3266. [PubMed: 24509865]

(38). Vural M; Behrens AM; Ayyub OB; Ayoub JJ; Kofinas P Sprayable Elastic Conductors Based on Block Copolymer Silver Nanoparticle Composites. ACS Nano 2015, 9, 336–344. [PubMed: 25491507]

(39). Kim Y; Zhu J; Yeom B; Di Prima M; Su XL; Kim JG; Yoo SJ; Uher C; Kotov NA Stretchable nanoparticle conductors with self-organized conductive pathways. Nature 2013, 500, 59–63. [PubMed: 23863931]

(40). Ma R; Lee J; Choi D; Moon H; Baik S Knitted Fabrics Made from Highly Conductive Stretchable Fibers. Nano Lett 2014, 14, 1944–1951. [PubMed: 24661242]

(41). Behrens AM; Lee NG; Casey BJ; Srinivasan P; Sikorski MJ; Daristotle JL; Sandler AD; Kofinas P Biodegradable-Polymer-Blend-Based Surgical Sealant with Body-Temperature-Mediated Adhesion. Adv. Mater 2015, 27, 8056–8061. [PubMed: 26554545]

(42). Medeiros ES; Glenn GM; Klamczynski AP; Orts WJ; Mattoso LHC Solution Blow Spinning: A New Method to Produce Micro- and Nanofibers from Polymer Solutions. J. Appl. Polym. Sci 2009, 113, 2322–2330.

(43). Srinivasan S; Chhatre SS; Mabry JM; Cohen RE; McKinley GH Solution spraying of poly(methyl methacrylate) blends to fabricate microtextured, superoleophobic surfaces. Polymer 2011, 52, 3209–3218.

(44). Jamnongkan T; Shirota R; Sukumaran SK; Sugimoto M; Koyama K Effect of ZnO Nanoparticles on the Electrospinning of Poly(vinyl alcohol) From Aqueous Solution: Influence of Particle Size. Polym. Eng. Sci 2014, 54, 1969–1975.

(45). Nikolova-Damyanova B Retention of lipids in silver ion highperformance liquid chromatography: Facts and assumptions. J. Chromatogr. A 2009, 1216, 1815–1824. [PubMed: 19027119]

(46). Ma R; Kang B; Cho S; Choi M; Baik S Extraordinarily High Conductivity of Stretchable Fibers of Polyurethane and Silver Nanoflowers. ACS Nano 2015, 9, 10876–10886. [PubMed: 26485308]

(47). Jiang S; Zhang H; Song S; Ma Y; Li J; Lee GH; Han Q; Liu J Highly Stretchable Conductive Fibers from Few-Walled Carbon Nanotubes Coated on Poly(m-phenylene isophthalamide) Polymer Core/Shell Structures. ACS Nano 2015, 9, 10252–10257. [PubMed: 26390200]

(48). Yu Z; Niu X; Liu Z; Pei Q Intrinsically stretchable polymer light-emitting devices using carbon nanotube-polymer composite electrodes. A. Mater 2011, 23, 3989–3994.

(49). Podsiadlo P; Kaushik AK; Arruda EM; Waas AM; Shim BS; Xu JD; Nandivada H; Pumplin BG; Lahann J; Ramamoorthy A; Kotovdv NA Ultrastrong and stiff layered polymer nanocomposites. Science 2007, 318, 80–83. [PubMed: 17916728]

(50). Lee KH; Kim HY; Ryu YJ; Kim KW; Choi SW Mechanical behavior of electrospun fiber mats of poly(vinyl chloride)/polyurethane polyblends. J. Polym. Sci., Part B: Polym. Phys 2003, 41, 1256–1262.

(51). Lee K; Lee B; Kim C; Kim H; Kim K; Nah C Stress-strain behavior of the electrospun thermoplastic polyurethane elastomer fiber mats. Macromol. Res 2005, 13, 441–445.

(52). Diani J; Fayolle B; Gilormini P A review on the Mullins effect. Eur. Polym. J 2009, 45, 601–612.

(53). Kluppel M; Schramm J A generalized tube model of rubber elasticity and stress softening of filler reinforced elastomer systems. Macromol. Theory Simul 2000, 9, 742–754.

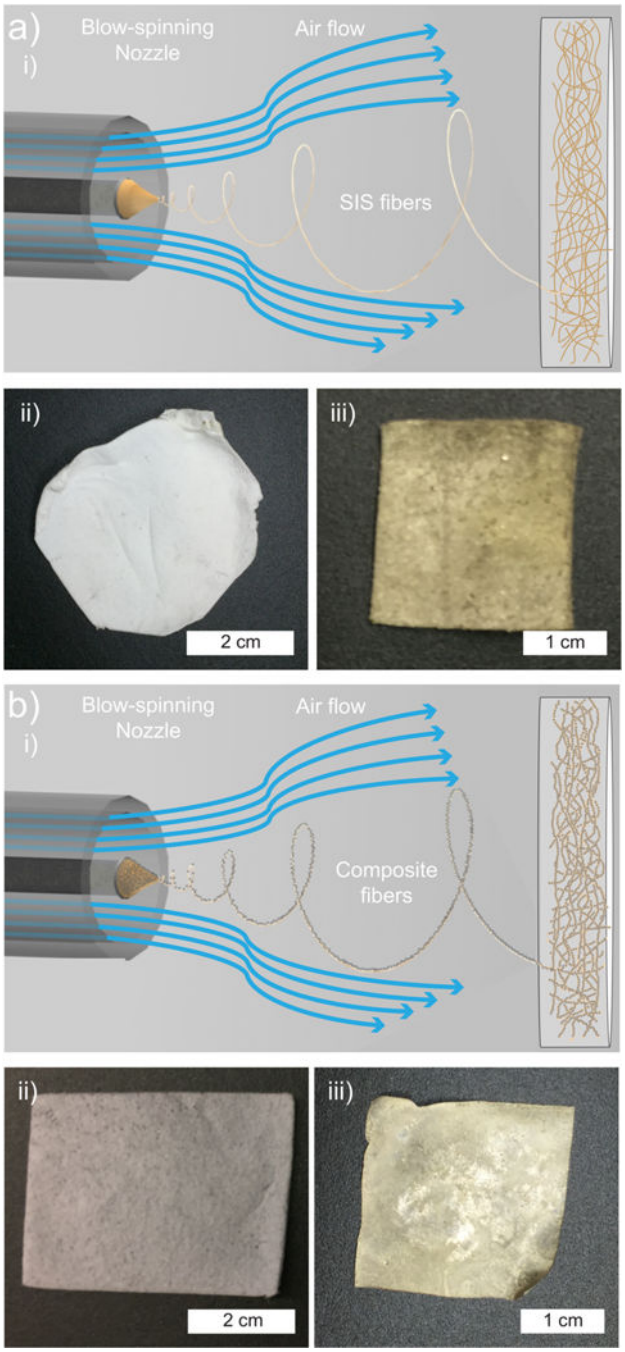

Figure 1.

(a) (i) Schematic illustration of solution blow spinning of SIS fiber mats. Images of (ii) nonconductive SIS fiber mat and (iii) elastic conductors fabricated using SIS fiber mat. (b) (i) Schematic illustration of solution blow spinning of composite fiber mats with Ag−PAA nanoparticles. Images of (ii) nonconductive composite fiber mat and (iii) elastic conductors fabricated using a composite fiber mat.

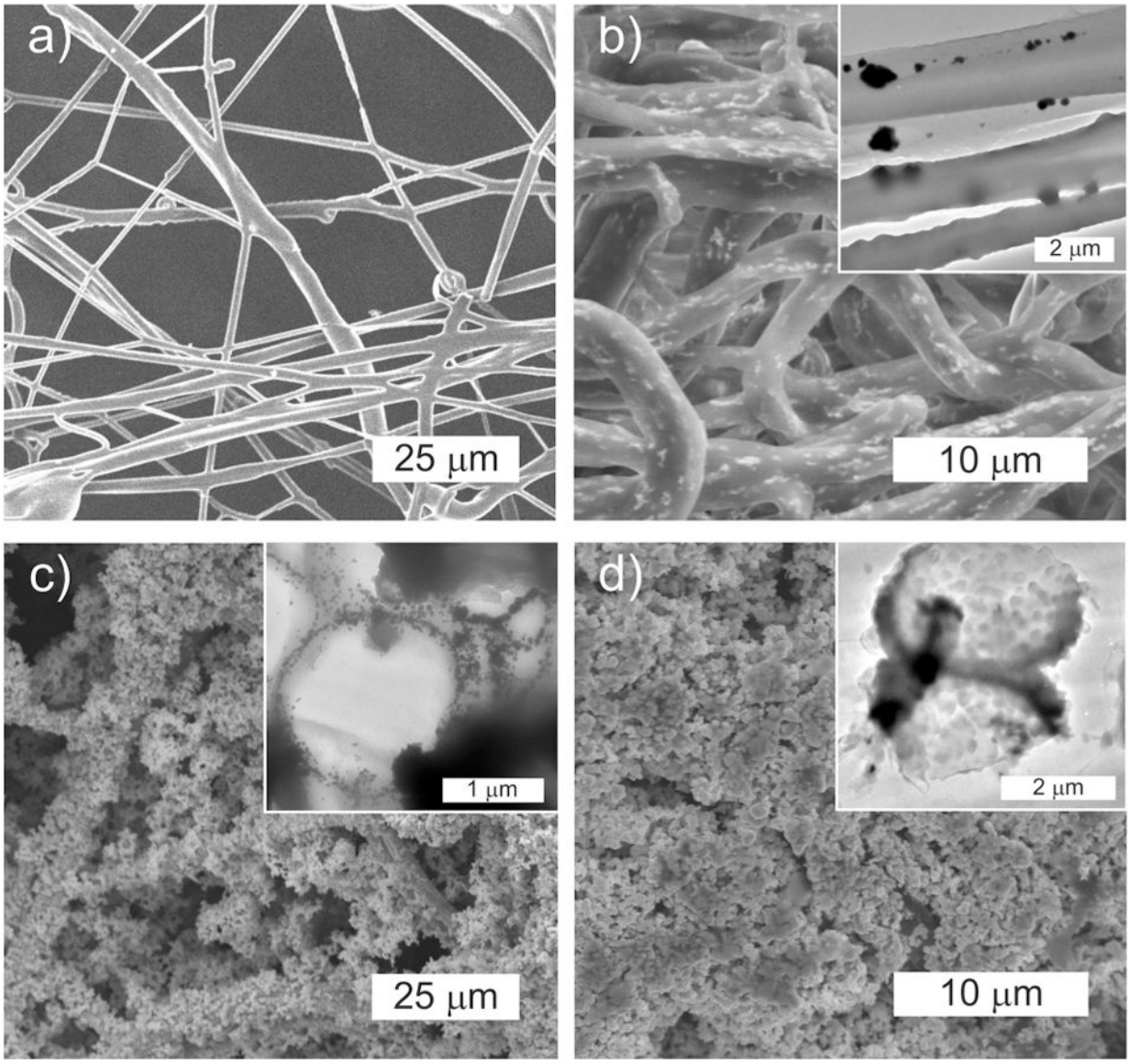

Figure 2.

SEM images of nonconductive (a) SIS fiber mat, (b) composite fiber mat, and elastic conductors fabricated using (c) SIS fiber mats and (d) composite fiber mats. TEM image of composite fiber mats (b, inset) and cross-sectional TEM images of elastic conductors fabricated using SIS fiber mats (c, inset) and composite fiber mats (d, inset) are provided as insets.

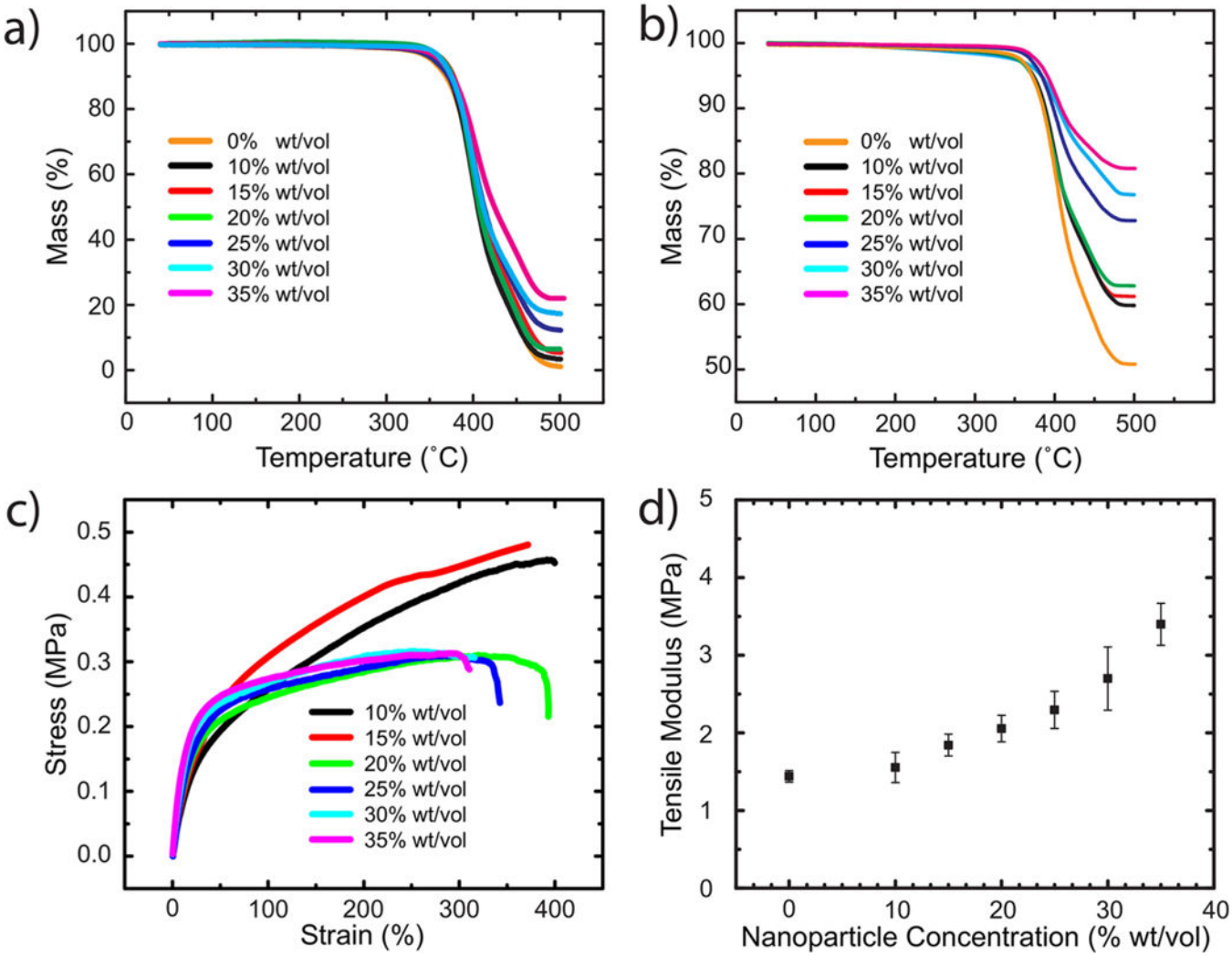

Figure 3.

Thermogravimetric analysis (TGA) of (a) nonconductive composite fiber network and (b) elastic conductors prepared with different concentrations of Ag−PAA nanoparticles in spinning solution. (c) Stress/strain curves and (d) tensile modulus of elastic conductors prepared using spinning solutions with different Ag−PAA nanoparticle concentrations (n = 6, error bars represent standard deviation).

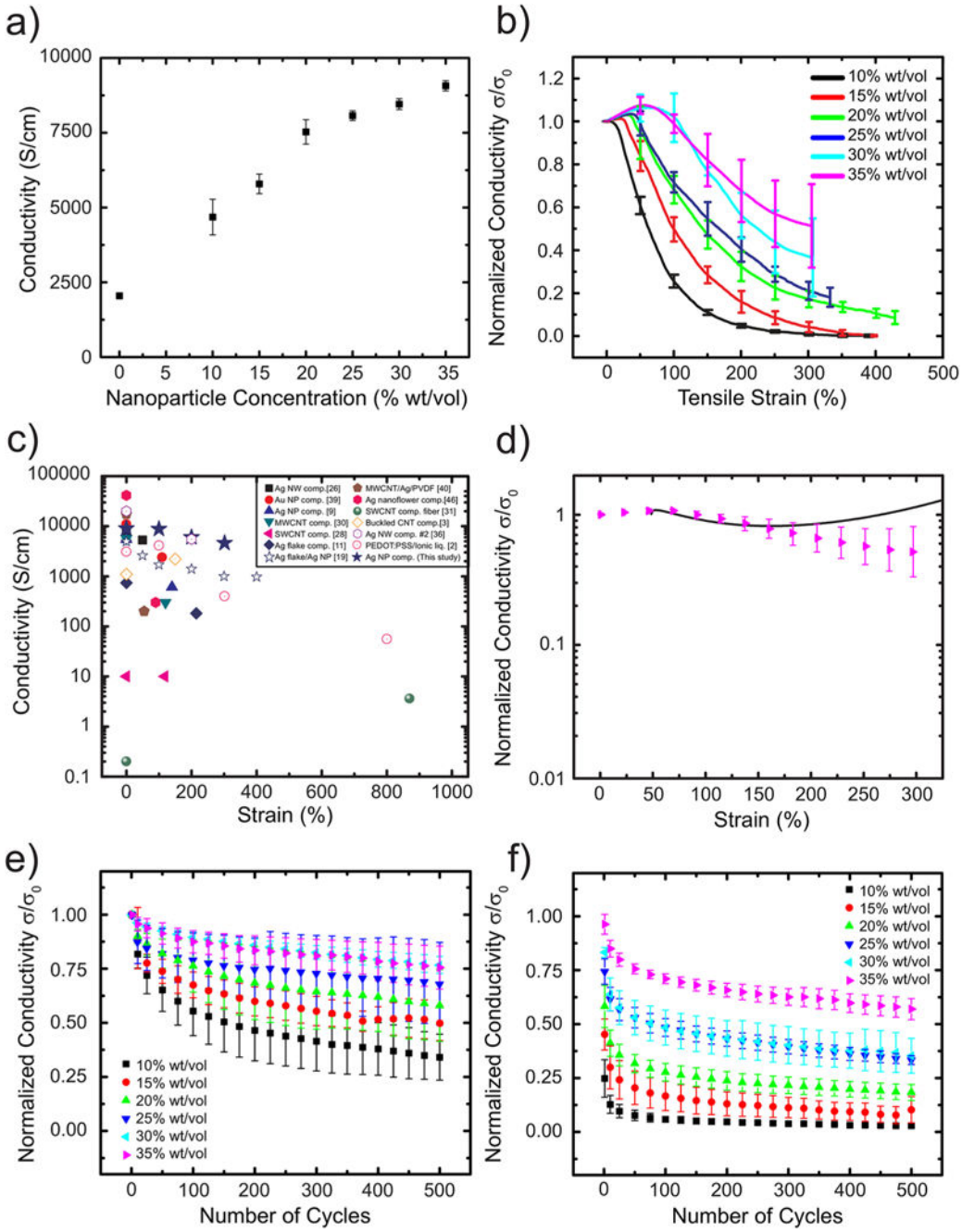

Figure 4.

(a) Electrical conductivity of elastic conductors prepared using spinning solutions with different Ag−PAA nanoparticle concentrations. (b) Normalized electrical conductivity (σ/σ_0) values for elastic conductors prepared using spinning solutions with different Ag−PAA nanoparticle concentrations under uniaxial tensile strain. (c) Comparison diagram of conductivity values under different strains for composites studied in this work and representative stretchable conductor reported previously. (d) Experimental (data points) and theoretical (eq 4) (black curves) normalized electrical conductivity (σ/σ_0) dependence on

strain for elastic conductors prepared using spinning solutions with 35% (w/v) Ag−PAA nanoparticle concentration under uniaxial tensile strain. Normalized electrical conductivity values at (e) released state (0% strain) and (f) stretched state (100% strain) for elastic conductors prepared using spinning solutions with different Ag−PAA nanoparticle concentrations as a function of cycle number (n = 3 for all groups, error bars represent standard deviation).

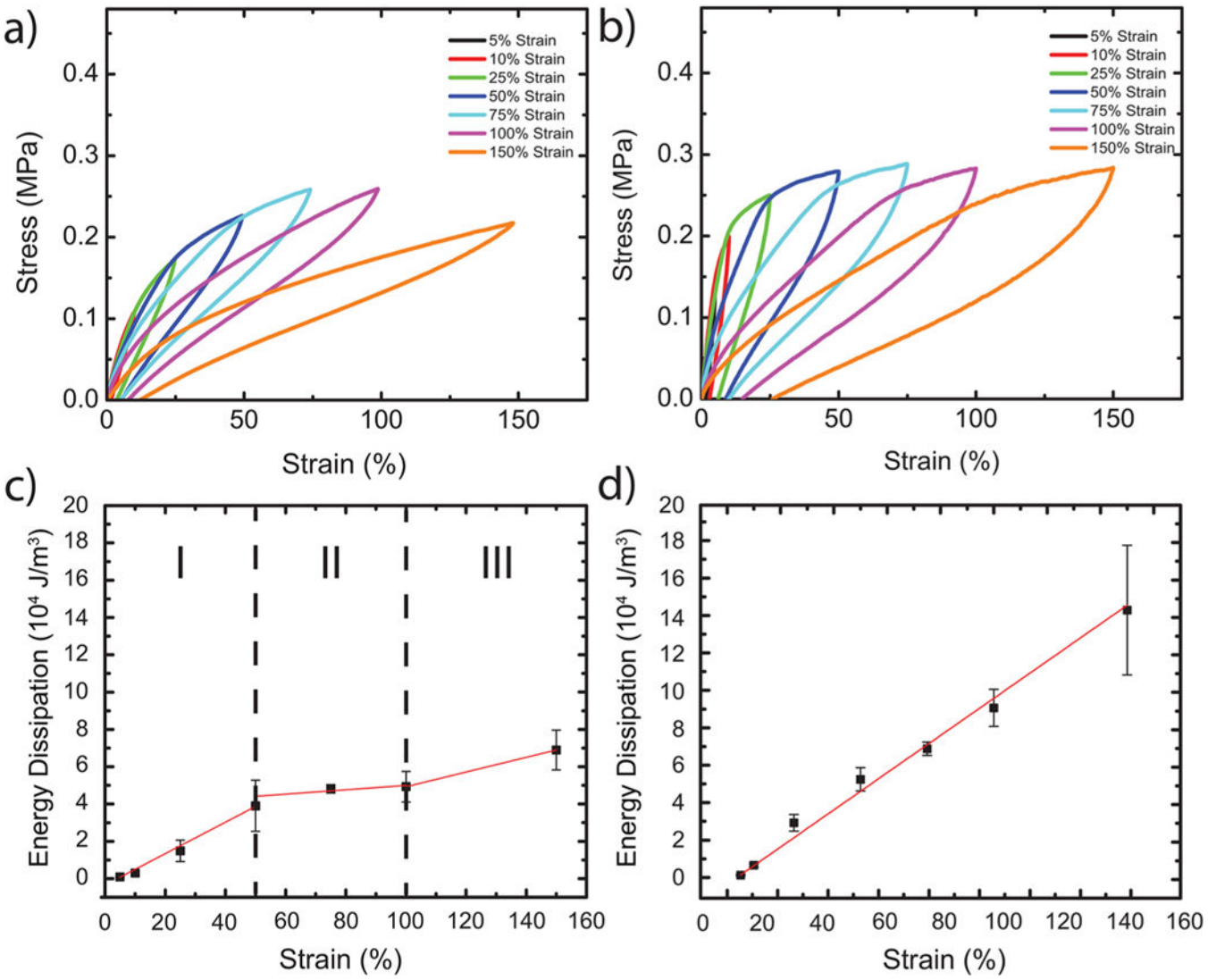

Figure 5.

Stress/strain cycling curves for elastic conductors prepared using spinning solutions with (a) 10% w/v and (b) 35% w/v Ag−PAA nanoparticle concentration. Average energy dissipation values and corresponding linear fits for elastic conductors prepared using spinning solutions with (c) 10% w/v and (d) 35% w/v Ag−PAA nanoparticle concentration (n = 3 for energy dissipation data, error bars represent standard deviation).

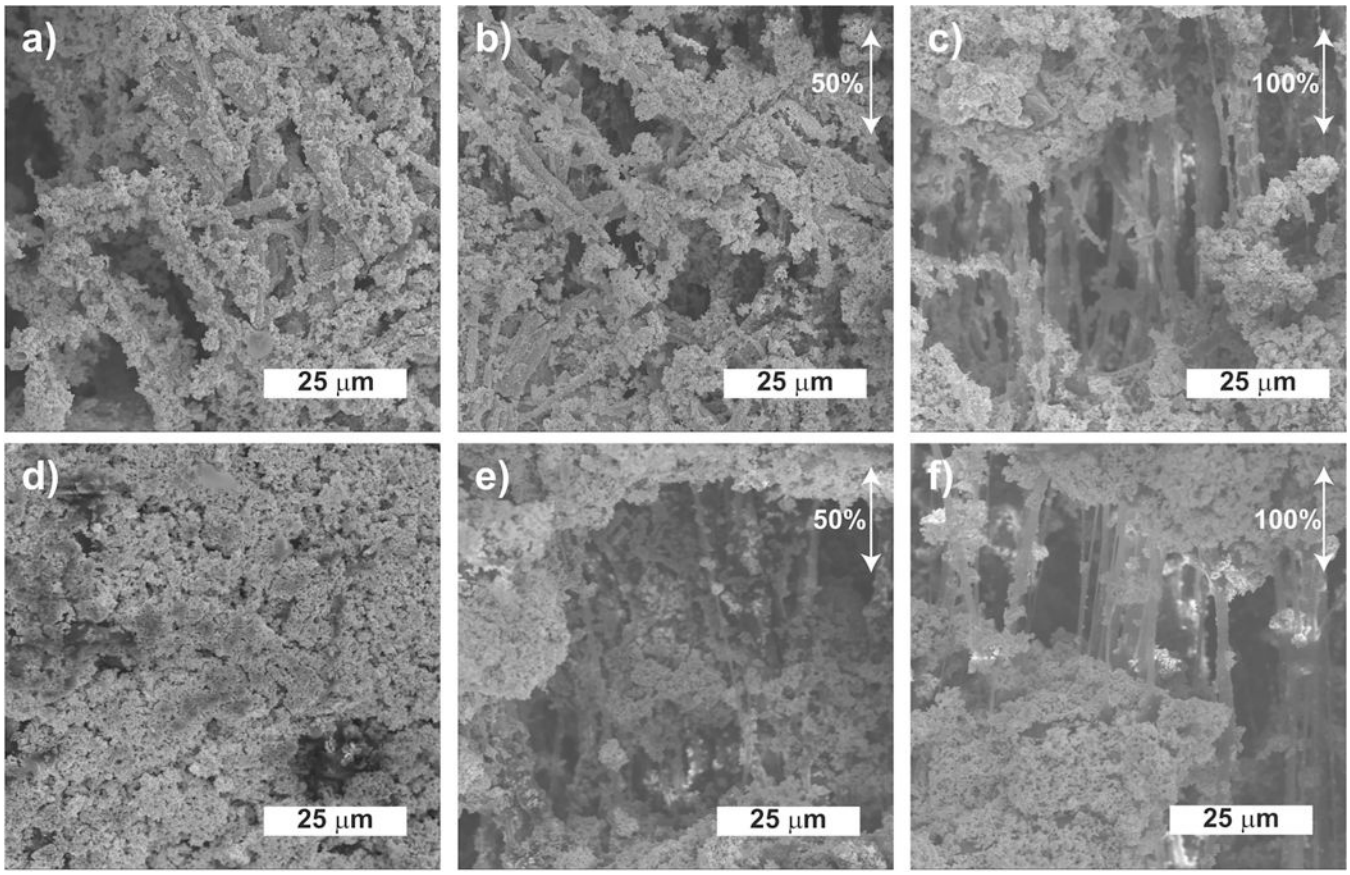

Figure 6.

SEM images of elastic conductors prepared using spinning solutions with 10% w/v Ag−PAA nanoparticle concentration under (a) 0% strain, (b) 50% strain, and (c) 100% strain. SEM images of elastic conductors prepared using spinning solutions with 35% w/v Ag−PAA nanoparticle concentration under (d) 0% strain, (e) 50% strain, and (f) 100% strain. The arrows indicate the direction of uniaxial tensile strain.